Title

Reversible Changes in the Grain Structure and Conductivity in a Block Copolymer Electrolyte

Journal

Macromolecules, 53(13)

ISSN

0024-9297

Authors

Chakraborty, Saheli
Jiang, Xi
Hoffman, Zach J
et al.

Publication Date

2020-07-14

DOI

10.1021/acs.macromol.0c00466

Peer reviewed

Reversible changes in grain structure and conductivity in a block copolymer electrolyte

Saheli Chakraborty[a], Xi Jiang[b], Zach J. Hoffman[c,e], Gurmukh K. Sethi[b,d], Chenhui Zhu[f] , Nitash P. Balsara*[a,c,d,e], Irune Villaluenga*[e]

[a]*Energy Storage & Distributed Resources Division, Lawrence Berkeley National Laboratory, Berkeley, California 94720, USA*

[b]*Materials Sciences Division, Lawrence Berkeley National Laboratory, Berkeley, California 94720, USA*

[c]*Joint Center for Energy Storage Research (JCESR), Lawrence Berkeley National Laboratory, Berkeley, California 94720, USA*

[d]*Department of Materials Science and Engineering, University of California, Berkeley, California 94720, USA*

[e]*Department of Chemical and Biomolecular Engineering, University of California, Berkeley, California 94720, USA*

[f]*Advanced Light Source, Lawrence Berkeley National Lab, California 94720, USA*

* Correspondence to: nbalsara@berkeley.edu and irvillaluenga@gmail.com

TOC graphic

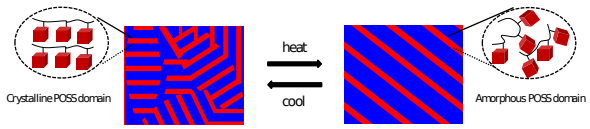

Abstract

We study the phase behavior of a triblock organic-inorganic hybrid copolymer, poly(polyhedral oligomeric silsesquioxane)-*b*-poly(ethylene oxide)-*b*-poly(polyhedral oligomeric silsesquioxane) (POSS-PEO-POSS)/ lithium bis(trifluoromethanesulfonyl) imide salt mixture as a function of temperature. The polymer exhibits a lamellar morphology, both in the neat state as well as in the presence of salt. However, the average grain size increases substantially when the electrolyte is heated above 113 °C. The grain structure of this sample changes reversibly with temperature, i.e., smaller grains reappear when the electrolyte is cooled below 113 °C. While annealing block copolymers at high temperatures often leads to an increase in grain size, this change is generally irreversible. The reason for the reversible change in the grain structure of the POSS-PEO-POSS/LiTFSI electrolyte is discussed. The ionic conductivity of the electrolyte also exhibits reversible changes in this temperature window. Knowledge of the grain structure is crucial for understanding ion transport in nanostructured electrolytes.

Introduction

Nanostructured block copolymer electrolytes are promising candidates for rechargeable batteries with high energy density lithium metal anodes.[1-4] These copolymers can microphase separate into ordered geometries with soft ion-conducting domains and mechanically rigid non-conducting domains, thereby enabling independent control over electrical and mechanical properties.[5,6] Ion transport in these materials is governed by geometry and connectivity of the conducting domains.[7] The geometry of the conducting domains is dictated by the thermodynamics of self-assembly.[8-18] The most commonly studied ordered geometry comprises alternating conducting and non-conducting lamellae. Coherent order in quiescently ordered block copolymers is limited to grains and macroscopic samples are made up of randomly oriented grains with concomitant defects and grain boundaries.[19-21] It has been shown that higher conductivity is obtained in samples with smaller grains.[22,23] Transport of ions across the grains depends on the nature of defects and hence is a complex function of grain structure.[24,25]

The grain structure of block copolymers is affected by both thermodynamics and kinetics. Defects and grain boundaries are trapped high free energy structures created during processing. Annealing samples generally leads to an irreversible increase in grain size due to processes such as defect annihilation.[26-28] In the block copolymer electrolyte studied thus far, this results in an irreversible decrease in conductivity.[22]

In this context, most of the copolymers studied thus far comprise all organic ion-conducting and non-conducting blocks. Recently, we demonstrated that electrolytes based on organic-inorganic hybrid diblock copolymers, poly(ethylene oxide)-*b*-poly(polyhedral oligomeric silsesquioxane) (PEO–POSS), exhibit superior mechanical properties relative to their all organic counterparts of comparable molecular weight.[29] The effect of grain structure on ionic

conductivity on this class of electrolytes has not been studied. In this article, we study an organic-inorganic hybrid triblock copolymer poly(polyhedral oligomeric silsesquioxane)-*b*-poly(ethylene oxide)-*b*-poly(polyhedral oligomeric silsesquioxane) (POSS-PEO–POSS). The electrolyte was prepared by mixing POSS-PEO-POSS with lithium bis(trifluoromethanesulfonyl)-imide (LiTFSI) salt. We show that this block copolymer electrolyte exhibits a reversible change in grain structure as a function of temperature. We describe our efforts to uncover the reason for this unexpected behavior and explore the relationship between grain structure and ionic conductivity.

Experimental Section:

Materials:

Polyethylene glycol (PEO) (M.W. = 10 kg/mol), α-Bromoisobutyryl bromide, trimethylamine, cupric bromide, N,N,N′,N″,N″-Pentamethyldiethylenetriamine (PMDETA), anhydrous tetrahydrofuran (THF) and toluene was purchased from Sigma-Aldrich. acryloisobutyl polyhedral oligomeric silsesquioxane (POSS) was purchased from Hybrid Plastics. Lithium bis(trifluoromethanesulfonyl)-imide, $Li[N(SO_2CF3)_2]$ (LiTFSI), was purchased from Novolyte. All the chemicals were used without further purifications.

NMR spectra:

^1H NMR spectra of the polymer was recorded using Bruker AV400 spectrometer. The samples were dissolved in deuterated chloroform containing tetramethylsilane (TMS) as internal standard.

Gel permeation chromatography

The molecular weight of the polymer was determined by gel permeation chromatography (GPC) using Agilent 1260 Infinity Series instrument, fitted with Waters Styragel HR 3 and 4 columns. N-Methyl-2-Pyrrolidone (NMP) containing 0.05M LiBr was used as the mobile phase and the experiment was conducted at 70 °C. The molecular weight was calibrated using PEO standards (Fluka). Due to

complex architecture of the polymer and poor solubility of the POSS segment in NMP, the GPC was only utilized to confirm the formation of block copolymer and estimating the PDI. The molecular weight was determined by NMR spectra.

Synthesis of polyethylene oxide macroinitiator:

10 g (1 mmol) of PEO (M.W. = 10 kg/mol) and 0.7 mL (5 mmol) of triethylamine was dissolved into 100 mL of anhydrous THF in a 250 mL round bottom flask. The mixture was then cooled in an ice bath and 0.5 mL (4 mmol) of α-Bromoisobutyryl bromide was added dropwise. The reaction mixture was allowed to stir at room temperature for next 8 hours. After that, the white precipitate was removed by filtration. The filtrate was concentrated and pure product was obtained by reprecipitating twice from diethyl ether (100X2 mL).

NMR (400 MHz, δ ppm, CDCl3): 4.32 (4H, -COOC**H_2**$CH_2OCH_2CH_2$-), 3.64 (906H, -$COOCH_2CH_2O$**CH_2CH_2**O-), 1.94 (12H, -COOC(**CH_3**)$_2$Br)

Synthesis of triblock copolymer POSS-PEO-POSS:

4 g (0.4 mmol) of the PEO-ATRP initiator and 16 g (17 mmol) of POSS-acrylate was added in 30 mL of degassed toluene. A 5 cm long Cu wire was washed thoroughly in methanolic HCl and added to the reaction mixture along with 4.5 mg (0.02 mmol) of $CuBr_2$. The mixture was purged with nitrogen for next 20 minutes. Finally, 40 µL of PMDETA was added and the mixture was heated at 60 °C for 20h under nitrogen atmosphere. After the reaction, it was diluted with 50 mL of THF and excess copper salt was removed by passing the solution through activated aluminium oxide. The filtrate was concentrated and reprecipitated three times from cold diethyl ether to obtain pure polymer as a white solid. The polydispersity index (PDI) is 1.09. Molecular weight based on NMR calculation is 13,700 kg/mol.

NMR (400 MHz, δ ppm, CDCl3): 3.64 (906H, -$COOCH_2CH_2O$**CH_2CH_2**O-), 0.94 (168H, -$SiCH_2CH$(**CH_3**)$_2$), 0.59 (64H, -Si**CH_2**$CH(CH_3)_2$)

Preparation of electrolytes:

The electrolytes of POSS-PEO-POSS and PEO were prepared by dissolving required amount of LiTFSI salt in the polymer. Due to the hygroscopic nature of

LiTFSI salt, the electrolyte preparation was carried out in an argon filled glove box (MBraun), where the H_2O and O_2 level were maintained at 0.5 ppm and 0.2 ppm, respectively. At first, the neat polymers were dried inside the glove box antechamber for 24 h at 90 °C. The LiTFSI salt was dried at 120 °C for 72 h under active vacuum. The dry polymer and LiTFSI salt were then dissolved in anhydrous THF and the solution stirred at 60 °C for at least 12 h in a capped vial. Once the solutes dissolved completely, the cap of the vial was removed to evaporate the THF at 60 °C for the next 12 h. Finally, the electrolyte was dried at the glove box antechamber for 72 h at 90 °C under active vacuum.

The salt concentration of the copolymer/salt mixture represented by r, the molar ratio of lithium ions to ethylene oxide (EO) moieties ([Li]/[EO]). The electrolytes used in this study have salt concentration, $r = 0.02$.

Differential scanning calorimetry (DSC):

Thermal properties of neat POSS-PEO-POSS and the electrolytes ($r = 0.02$) was determined by DSC. 5-7 mg of the samples were placed in a TZero aluminum pan and sealed with a TZero hermetic lid (T.A. Inc) inside the argon glove box. The experiment was performed with two heating and two cooling runs using Thermal Advantage Q200 calorimeter at the Molecular Foundry, LBNL. The temperature range for the experiment lies between -80 °C to 150 °C with the heating rate of 10 °C/min and cooling rate of 2 °C/min. The melting point and glass transition temperatures were determined by analyzing the second heating curve.

Small angle X-ray Scattering (SAXS):

The morphology of the polymer and the electrolyte was determined by small angle X-ray scattering (SAXS) experiments. The samples were prepared in a 1 mm thick annular Viton rubber spacer (McMaster Carr) with an internal diameter of 1/8 inch by hot pressing at 120 °C. It was then sealed with Kapton windows in custom-designed airtight aluminum sample holders within the glove box. The samples were annealed at 120 °C for 24 h before taking to the beamline.

The SAXS measurements were conducted at the Advanced Light Source beamline 7.3.3 at Lawrence Berkeley National Lab and Stanford Synchrotron Radiation Light Source beamline 1-5 at SLAC National Accelerator Laboratory. Silver behenate was used to determine the beam center and the sample-to-detector distance. The samples were mounted in a custom build 8-sample hot stage. The samples were heated from room temperature in a stepwise manner to 140 °C (90 – 110 – 140 °C), annealed at each temperature for 20 minutes expect at 90 °C where they were annealed for 30 minutes. The samples were then cooled to 90 °C in a stepwise manner (130 – 120 – 110 – 100 – 90 °C), annealing these cells for 20 minutes at each temperature. The actual temperatures of the samples were reported based on the temperature calibration curve. The two dimensional scattering patterns were obtained at each temperature during both the heating and cooling runs. These scattering patterns were azimuthally averaged using the Nika program for IGOR Pro[30] to produce the one-dimensional scattering profiles; all two dimensional profiles were azimuthally symmetric. The SAXS intensity, I, is reported as a function of the magnitude of the scattering vector, q; where,

$$q = 4\pi\sin(\theta/2)/\lambda \qquad (1)$$

where θ is the scattering angle, and λ is the wavelength of the X-rays which is equal to 1.2398 Å.

Wide angle X-ray Scattering (WAXS):

The samples for WAXS studies are prepared exactly same way as that of the SAXS studies. The WAXS measurements were done at Advanced Light Source beamline 7.3.3 at Lawrence Berkeley National Lab. The samples were in a custom build 8-sample hot stage. During the experiment the samples were heated from room temperature to 150 °C in a stepwise manner (90 – 120 – 150 °C) and cooled to 90 °C in a stepwise manner (120 – 90 °C) and annealed for 20 minutes at each temperature. The scattering images were captured using a sample to detector distance of 30.84 cm. Silver behenate was used to determine the beam centre and the sample-to-detector distance. The scattering patterns were analysed using the Nika program for IGOR Pro[30]. The actual temperatures were reported based on the temperature calibration curve.

Transmission electron microscopy:

The electrolyte samples was prepared in the aluminium holders as described in the preparation of SAXS samples. The holders were then heated to the desired temperatures on a hot plate for 20 minutes. The samples were then quenched in liquid nitrogen for 10 minutes before bringing to the room temperature. The electrolytes were sectioned at -120 °C using cryo-microtome (Leica Ultracut 6) to obtained ultrathin films (~100 nm). The films were then transferred on to copper grids coated with lacey carbon supported films and transferred immediately inside the glove box to prevent absorption of moisture. The electrolytes were stained with ruthenium tetroxide for 10 minutes to improve the contrast. High-angle annular dark-field scanning transmission electron microscopy (HAADF-STEM) micrographs were collected using FEI Tecnai F20 at 200 kV with camera length 140 cm.

Rheology:

The viscoelastic properties were studied using a strain-controlled Rheometric Scientific ARES (Advanced Rheometric Expansion System) rheometer. The rheometer was equipped with 8 mm diameter parallel plates. The samples were prepared in a 1 mm thick rubber spacer with internal diameter of 8 mm via hot pressing at 120 ^{o}C for 24 h in order to get rid of any air bubbles. The temperature dependent viscoelastic behavior was determined by a temperature sweep test between 70 ^{o}C to 130 ^{o}C with a frequency of 1 rad/s and a strain of 0.1%.

Impedance spectroscopy:

The stainless steel symmetric cells were prepared to measure the conductivity of the electrolyte. The electrolyte was hot pressed into a silicon spacer of 254 µm thickness and 3.175 mm diameter hole and was sandwiched between 200 µm thick stainless-steel shim blocking electrodes. The silicon forms a good seal to prevent the leakage of the electrolyte. Aluminium tabs were secured to the stainless steel electrodes to provide electrical contacts. The whole assembly was hermitically sealed in a Showa-Denko pouch material with only the tab ends exposed. This assembly allows us to perform measurement

outside the glove box while maintaining a moisture and air free environment. The complex impedance were performed using Bio-Logic VMP3 potentiostat over a 0.1–10^6 Hz frequency range at an amplitude of 80 mV. The standard protocol for determining the conductivity of the POSS-PEO-POSS/LiTFSI electrolytes is as follows. The pouch cells were heated to 120 °C in a stepwise manner (30 – 50 – 70 – 90 – 110 – 120 °C), annealing the cells at each temperature for 30 minutes except for 90 °C anneal which was performed for 3 hrs. The cells were then cooled to 30 °C in a stepwise manner (110 – 70 – 50 – 30 °C), annealing these cells for 20 minutes at each temperature. This was followed by a second heating run (from 30 to 100 °C in 10 °C steps and between 100 to 130 °C in 5 °C steps). The thermal history used for the impedance experiments is similar but not identical to that used in the SAXS experiments. (Limited access to SAXS beam time precludes taking 5 °C steps.) The measurements were repeated with six independent cells and the standard deviation was used to estimate the error bars. The cells were opened inside the glovebox after the experiments to measure the final thickness.

Results and discussion:

The small angle X-ray scattering (SAXS) profiles of the neat POSS-PEO-POSS copolymer in the temperature range of interest (between 94 and 122 °C) is shown in Figure 1a. Here, the scattering intensity I, is plotted against the magnitude of the scattering vector, q. Figure 1a shows SAXS profiles of neat POSS-PEO-POSS obtained during the cooling run. The polymer exhibits a lamellar morphology at 94 and 103 °C. This is evident due to the presence of the primary scattering peak at $q = q^* = 0.387$ nm^{-1}, and higher order peaks at $2q^*$ and $3q^*$. The domain spacing of the ordered morphology, defined as

$$d = 2\pi / q^* \qquad (2)$$

is equal to 16.2 nm. At 113 °C, the intensities of the primary scattering peak and the higher order peaks decrease sharply. However, sharp peaks indicative of an ordered phase are present even at high temperatures. We conclude that the abrupt decrease in SAXS intensity seen at 113 °C is due to an abrupt change in scattering contrast between the lamellae. We will return to this point shortly. Figure 1b shows the scattering profiles of the POSS-PEO-POSS/LiTFSI $r = 0.02$ electrolyte during a cooling run. Here we see a sharp primary scattering peak at

all temperatures. At 94 and 103 °C, we observe higher order scattering peaks at 3q* and 4q*. At 113 and 122 °C, the primary scattering peak is sharper, and we observe a new peak at 2q*; the 3q* and 4q* peaks are not present at these temperatures. The value of d obtained from the electrolyte is 17.5 nm at all the temperatures shown in Figure 1b.

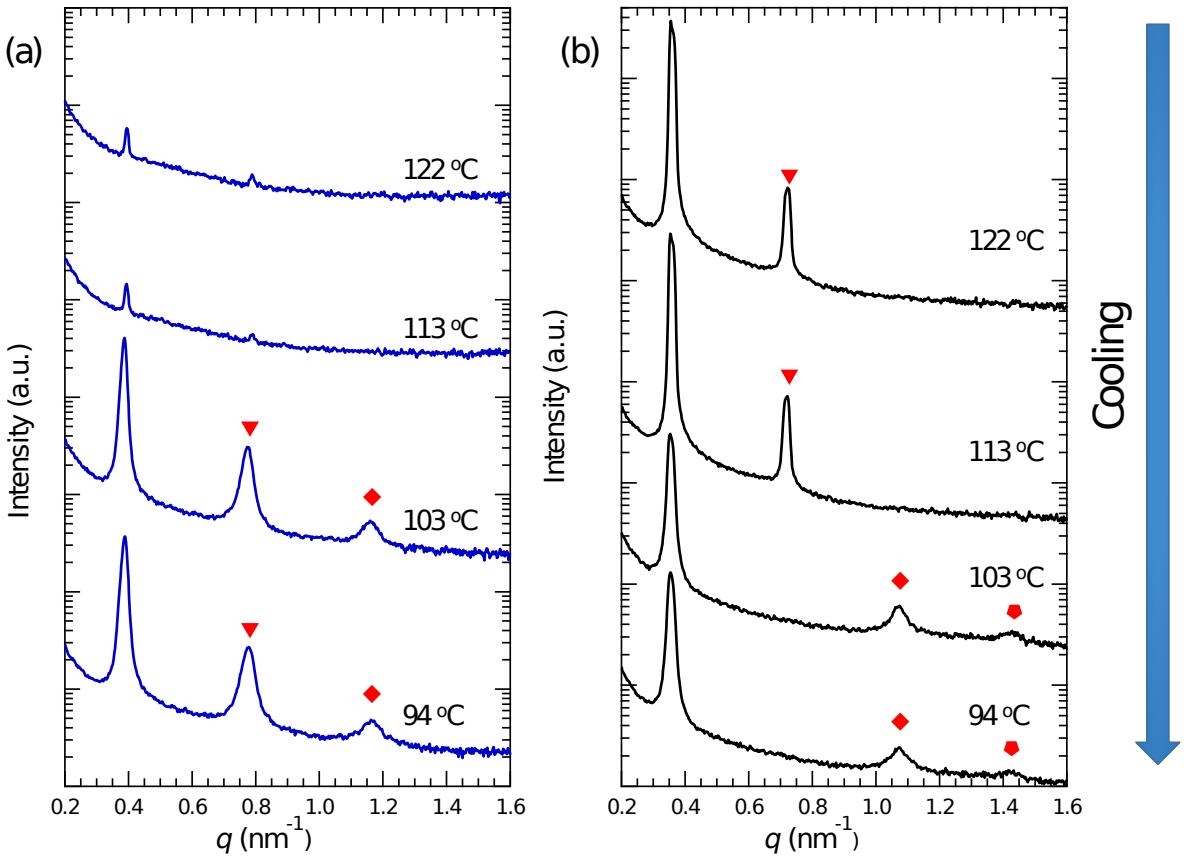

Figure 1. Scattering intensity I of POSS-PEO-POSS is plotted as a function of the scattering vector, q, at various temperatures for (a) neat POSS-PEO-POSS and (b) POSS-PEO-POSS/LiTFSI electrolyte with r = 0.02. The profiles are shifted vertically for clarity. The triangles, rhombus and pentagon represents the second, third and fourth order peaks, respectively.

The data shown in Figure 1 were obtained during a cooling run. We also conducted heating runs and found similar behavior as shown in Figure 1. For brevity, we do not show the heating data from neat POSS-PEO-POSS. The reversible nature of the SAXS data for the electrolyte is more interesting. The effect of thermal history on SAXS profiles of the electrolyte is shown in Figure 2. The electrolyte was heated from room temperature to 103 °C and the SAXS

profile thus obtained is shown in Figure 2. We see broad peaks at q^* and $3q^*$. The value of d in this sample is 15.7 nm and the SAXS peak is significantly broader than that obtained during the subsequent cooling run at the same temperature; compare 103 °C data in Figures 1b and 2. In addition, the domain spacing is also significantly smaller during the heating run. Further increase in the sample temperature to 131 °C results in the disappearance of the $3q^*$ peak and appearance of the $2q^*$ peak. Cooling the sample back down to 103 °C results in a SAXS profile with peaks at q^*, $3q^*$, and $4q^*$.

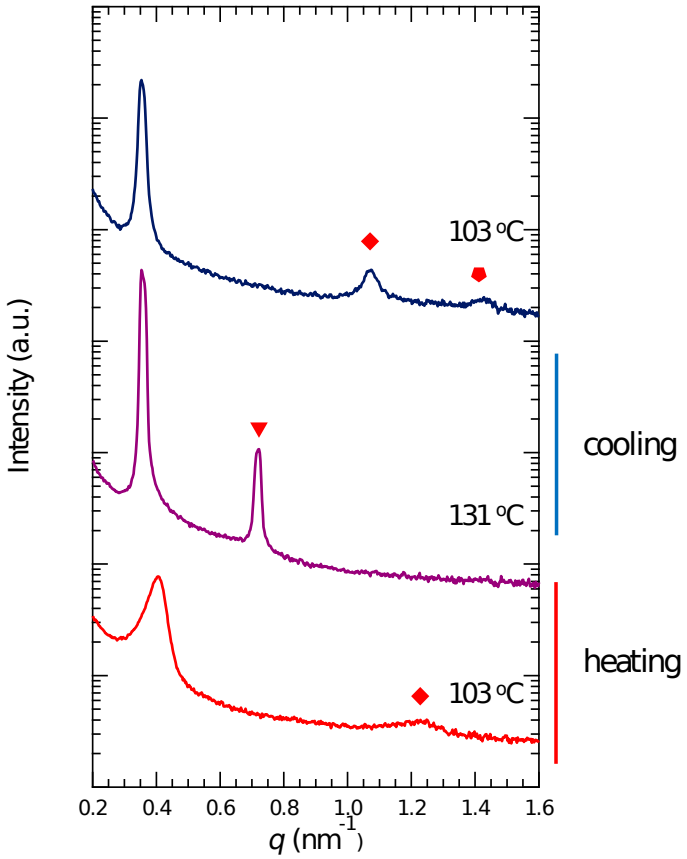

Figure 2. The scattering intensity is plotted against the scattering vector, q, for three temperatures for the electrolyte. The SAXS pattern indicates the reversibility of heating and cooling scans. The triangle, rhombus and pentagon represent peaks at $q = 2q^*$, $3q^*$, and $4q^*$, respectively

The width of the primary SAXS peak depends on both intra-grain and inter-grain effects.[31] The evidence that subtle changes in grain structure and connectivity have a significant effect on ion transport equation[32,33] applies to the simple case where peak width is primarily affected by the average grain size; the

order within individual grains is assumed to be same. In ordered block copolymers, the order within each grain is affected by complex factors such as local lamellar undulations and the width of the interface between adjacent lamellae. We will present evidence to show that the local order on length scales comparable to d is, to a large extent, unaffected by thermal history. We thus define a length scale, L, that is a measure of the average grain size, $L = 2\pi K(\text{fwhm})^{-1}$ according to the Scherrer equation, where fwmh is the full width at half maximum of the primary SAXS peak, and K is a constant that we take to be 0.93 as given in reference 33. The primary SAXS peak was fit to a Gaussian profile after background subtraction and fwhm was calculated from the fit. Figure 3a shows the dependence of L on temperature. It is clear that L increases sharply during the heating run. Upon subsequent cooling, L decreases substantially, but it does not match the value obtained during the heating run.

The scattering invariant, S, is defined as,

$$S = \int_{q1}^{q2} I q^2 dq \quad . \qquad (3)$$

We computed S for the primary peak in the electrolyte according to Eq. 3 with $q_1 =$ ¿ 0.30 and q_2 = 0.45 nm^{-1}, after background subtraction. In Figure 3b we plot the ratio of $S_{T=T'} / S_{T=130}$, where T' is temperature of interest, as a function of temperature during heating and cooling cycles. It is evident that the invariant at 103 ºC is similar during both heating and cooling runs in spite of the qualitative differences in the SAXS profiles seen in Figure 2; the slight differences will be discussed below. Both the d spacing and fwhm of the primary scattering peak at 103 ºC differ considerably between the heating and cooling runs. However, the invariant is similar. This is because the sample is fully ordered at 103 ºC for both the heating and cooling runs. The data in Figure 2 and 3 indicate a reversible transition between two fundamentally different ordered phases. We conducted electron microscopy experiments to determine the distinction between the two phases.

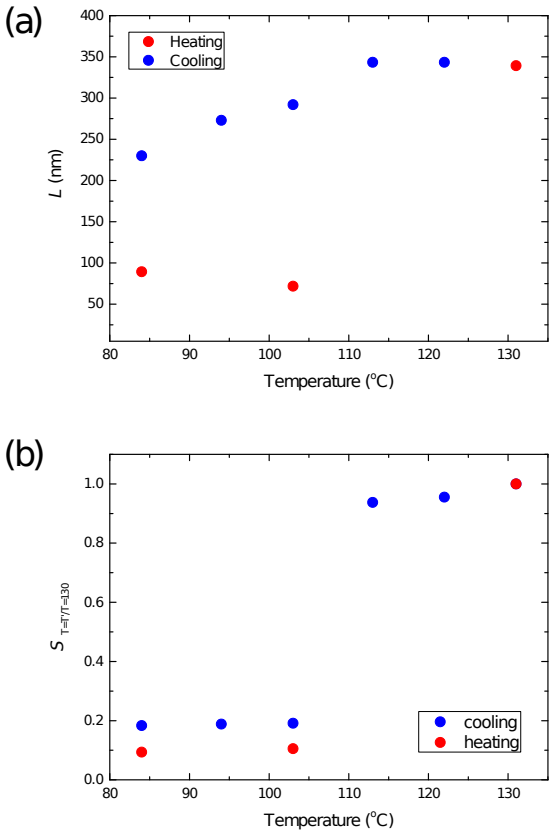

Figure 3. (a) The grain size (*L)* of the electrolyte is plotted as a function of temperature. (b) The ratio of scattering invariant $S_{T=T'}/S_{T=130}$ of the electrolyte is plotted against the experimental temperatures. The red and blue circles denote the heating and cooling cycles, respectively.

Two separate electrolyte samples were annealed at 100 and 130 °C, and quenched in liquid N_2 to freeze the morphologies at these two temperatures. The HAADF-STEM micrographs thus obtained are shown in Figure 4, where the bright regions represent the PEO domains, stained with RuO_4. At both the temperatures, the micrographs show the presence of alternating bright and dark stripes, corresponding to PEO-rich and POSS-rich lamellae, respectively. This shows that the local order on length scales comparable to the lamellar d-spacing is unaffected by thermal history. However, at 100 °C the micrograph contains several grains within which lamellar order is coherent, while at 130 °C we observe one large lamellar grain. The difference in long range order is clearly seen in the Fourier transforms of the micrographs. The Fourier transform of the 100 °C micrograph contains wide arcs arising from lamellae oriented in different

directions while that at 130 °C contains two sharp reflections. While there may be subtle differences in the intra-grain structures at 100 and 130 °C, the main difference between the morphologies is the extent of long-range order. The grain structure in any material is complex and difficult to quantify. Grains are irregularly shaped and different averages are determined by different techniques.[34] The particular grains shown in Figure 4 are larger than the average grain size determined by SAXS.

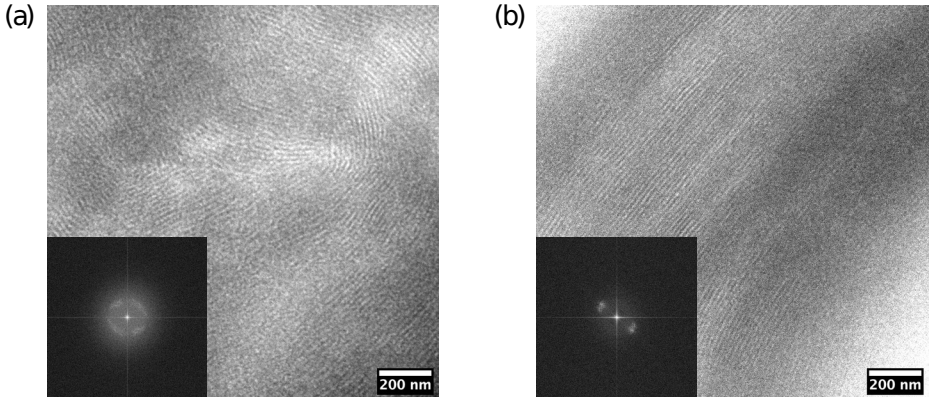

Figure 4. HAADF-STEM micrographs of the electrolyte annealed at (a) 100 °C and (b) 130 °C, respectively and quenched in liquid nitrogen. The bright phase represents RuO_4 stained PEO domains. The inset shows Fourier transform of the micrographs.

In order to understand the origin of the temperature-induced reversible change in grain structure, we examine the thermal behavior of the neat polymer and the electrolyte. Figure 5a shows the heating and cooling DSC traces of the electrolyte. The heating scan indicated melting of PEO domain at 50 °C and a second melting peak at 117 °C. Similarly, in the cooling scan an endothermic peak was detected at 107 °C along with a peak at 35 °C due to the crystallization of PEO. The neat POSS-PEO-POSS copolymer exhibits similar thermal behavior (Figure S6). We also conducted DSC experiment on the POSS homopolymer and the results are shown in Figure S8. The POSS homopolymer is semicrystalline with a melting temperature of around 150 °C. We thus attribute the higher temperature DSC peak in our electrolyte to melting and crystallization of the POSS-rich microphases[35,36]; the melting points of block copolymer microphases often occur at temperatures that are different from that of bulk samples.[37-41] The

enthalpy of melting of the POSS microphase in the POSS-PEO-POSS/LiTFSI electrolyte (15 J/g of POSS) is higher than that of POSS homopolymer (9 J/g of POSS).

In references 18 and 29, we have reported on the phase behavior of PEO-POSS/LiTFSI mixtures. The melting of POSS microphases was missed in those publications. It is likely that phase transitions reported in those studies in the vicinity of 120 °C are affected by this phenomenon. Work on re-evaluating the assessment of phase behavior in previous studies due to crystallinity of POSS domain is currently underway.

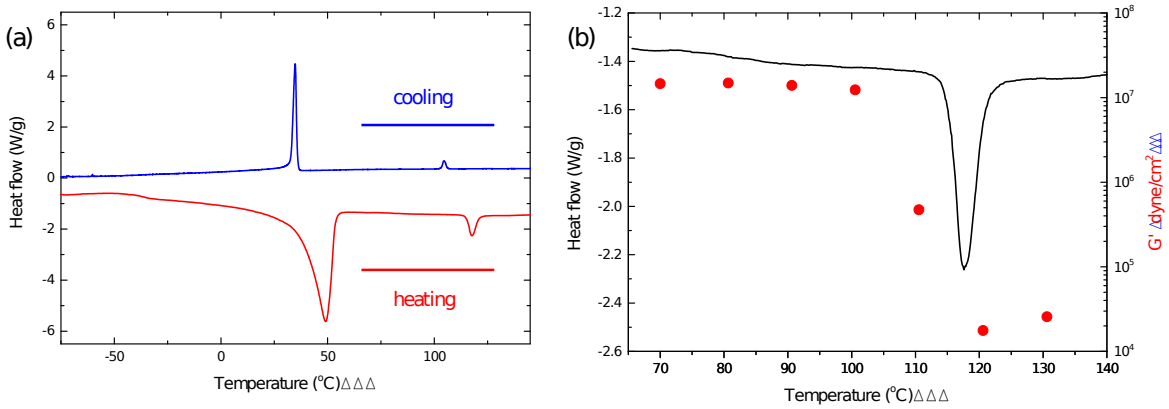

Figure 5. (a) DSC thermogram of the electrolyte indicating heat flow for heating (red) and cooling (blue) scans. (b) The storage modulus (red dot) (G') of the electrolyte is plotted against temperature. The black curve represents DSC thermogram. The storage modulus decreases sharply at the temperature at which the exothermic transition was noted in DSC thermogram.

The temperature dependence of the storage modulus of the POSS-PEO-POSS/LiTFSI electrolyte, at ω = 1 rad/s, is shown in Figure 5b. The melting of POSS results in a decrease of storage modulus (G') from 10^7 dyne/cm^2 at 110 °C to 2x10^4 dyne/cm^2 at 120 °C. It is clear that the rigidity of the electrolyte depends crucially on the crystallinity of the POSS microphase.

Wide angle X-ray scattering (WAXS) experiments were performed to confirm the melting of the POSS-rich microphase. Figure 6 shows the WAXS profiles from the POSS-PEO-POSS/LiTFSI electrolyte. At 84 °C, sharp scattering peaks were observed at q = 5.9, 8.0 and 13.8 nm^{-1}. These peaks correspond to the rhombohedral packing of the POSS moieties.[35,36] The PEO-rich microphase remains amorphous at these temperatures (Figure S11a). Upon heating at 141 °C the sharp peaks disappear and broad amorphous halos were obtained indicating the melting of POSS microphases. All the peaks reappear on cooling the sample to 84 °C.

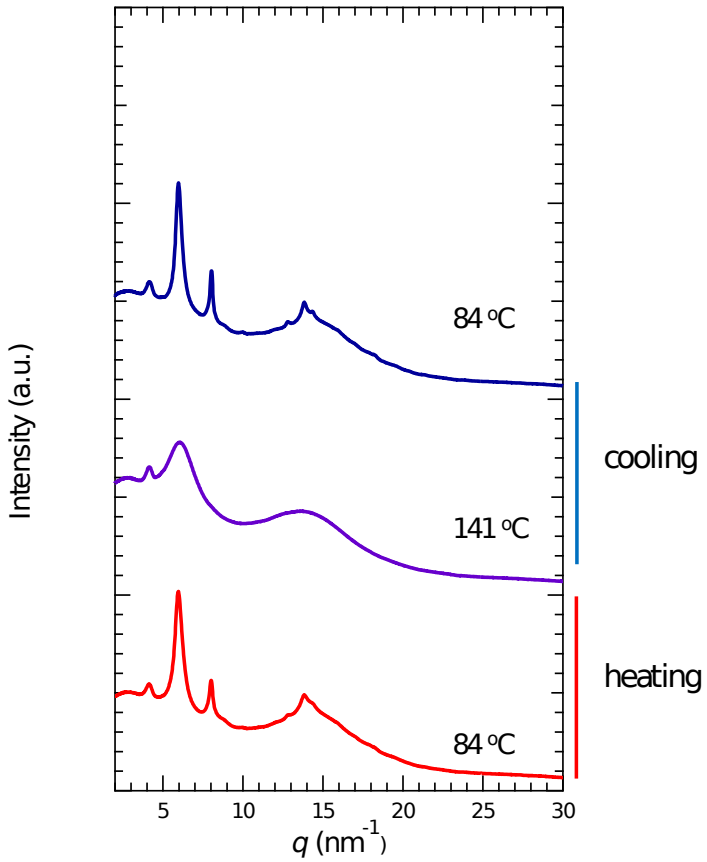

Figure 6. The WAXS pattern with scattering intensity is plotted against the scattering vector, q, for three temperatures for the electrolyte. The WAXS pattern indicates the melting and recrystallization of POSS microphases. The sharp peak at 4 nm^{-1} is due to kapton window (Figure S11b).

The reason for the reversible change in grain structure in the vicinity of 113 °C is now clear. At temperatures below 113 °C the POSS microphase is

semicrystalline and this crystallinity disrupts coherently ordered grains. Larger grains with much more pronounced coherent order are obtained above the melting temperature of the POSS microphase. This difference is established by SAXS (Figure 2) and TEM (Figure 4). The effect of crystallinity on ordered microphases in block copolymers is a subject of long-standing interest. For semicrystalline block copolymers, microphase separation is governed by either the block incompatibility or the crystallization of the blocks. Crystallization induces the formation of lamellar phases regardless of block copolymer composition due to the planar motif of polymer crystals.[42-45] Register and coworkers have established that crystallization can either be confined within the microphases or breakout of the microphases depending on the interblock segregation strength.[46] More recently it has been shown that in some cases for block copolymer electrolytes, crystallization can either occur in a manner that preserves the grain structure (in addition to preserving the microphase structure). We refer to this as confined crystallization. In other cases, the microphase structure is preserved but the grain structure is not. We called this case unconfined crystallization. [47] The electrolyte in this study exhibits an unconfined crystallization.

We posit that the abrupt change in the SAXS intensity in the neat POSS-PEO-POSS when the sample is heated from 103 to 113 °C is due to the melting of the POSS microdomains. Densities of polymers with or without salts change only slightly in a 10 °C window. In addition the electrolyte contains negligible amounts of LiTFSI. We can thus base our arguments on the densities of pure POSS and pure PEO which are 1.3 and 1.128 g cm^{-3} at 90 °C respectively. The POSS is crystalline at this temperature and the electron density contrast of POSS and PEO is calculated to be 0.025 cm^{-1}. A 12 % decrease in the density of POSS upon melting will lead to a decrease in scattering contrast by a factor of 115 (calculation shown in SI). The difference in SAXS invariant for POSS-PEO-POSS/LiTFSI between the heating and cooling runs at 85 °C in Figure 3b are also related to the crystallinity of POSS: POSS is a semicrystalline polymer and the crystalline fraction obtained during the cooling run will be lower than that obtained during the heating run. Further work is needed to determine the relevant densities necessary to accurately calculate the scattering contrast including effects such as the volume change of mixing. We note in passing that

the volume change of mixing in bulk PEO/LiTFSI mixtures has only recently been measured.[48]

We return to the SAXS profiles in Figure 1b. While the TEM, DSC and WAXS data provide an explanation for the disappearance of the second order SAXS peak at 94 and 103 °C, we have no definitive explanation for the appearance of broad third and fourth order SAXS peaks at these temperatures. We suggest that these peaks arise due to the complexity of the crystallized POSS lamellae. In the crystalline state, our sample comprises three phases: an amorphous PEO-rich phase and coexisting amorphous and crystalline regions within the POSS-rich lamellae. It has been shown that such systems can organize in complex geometries including trilayer morphologies and periodically spaced crystals within the lamellae.[49-53] The broad third and fourth order SAXS peaks could arise due to such morphologies. While some aspects of the morphology of the POSS-PEO-POSS/LiTFSI electrolyte remain unexplained, we have presented conclusive evidence for the fact that the system exhibits a reversible change in grain structure at 117±5 °C due to the melting of the non-conducting POSS-rich microdomains.

The effect of changes in the grain structure on conductivity were determined by ac impedance experiments. The temperature dependence of the conductivity of the electrolyte, obtained during the second heating run, as described in the Experimental Section, is shown in Figure 7a. The data points in Figure 7a represent averages over 6 independent cells. Also shown in the same figure is the conductivity of PEO (molecular weight = 10 kg/mol) at r = 0.02 as a function of temperature.

The conductivity of the electrolyte at different temperatures is affected by both changes in the conductivity of the PEO-rich microphase and changes in grain structure. To focus on the effect of grain structure we define a normalized conductivity κ_n as

$$\kappa_n = \frac{\kappa_{POSS-PEO-POSS}}{\kappa_{PEO} f_{EO/LiTFSI}} \qquad (4)$$

where, $\kappa_{POSS\text{-}PEO\text{-}POSS}$, κ_{PEO} and $f_{EO/LiTFSI}$ are the conductivity of the POSS-PEO-POSS/LiTFSI copolymer, PEO homopolymer and volume fraction of the conducting EO phase in POSS-PEO-POSS, respectively.

The temperature dependence of κ_n is shown in Figure 7b. The vertical bar in Figure 7b denotes the range of temperatures over which the POSS microphases melt. It is evident that, the increase in grain size in POSS-PEO-POSS/LiTFSI electrolytes due to melting of POSS, results in a decrease in κ_n. The observation that increase in grain size reduces conductivity is consistent with literature reports.[22,23]

In Figure 7c, we show conductivity data obtained from a particular cell that was subjected to four separate heating runs. The first and second heating runs were conducted in accordance with the standard protocol described in the Experimental Section. The red circles in Figure 7c, obtained during the second heating run, are entirely consistent with the data shown in Figure 7a. In fact, the cell described in Figure 7c is one of the six cells averaged in Figure 7a. The cell was then cooled in a stepwise manner with 5 °C steps down to 100 °C followed by a 10 °C step to 90 °C. The conductivity data obtained during this the cooling run, shown by blue circles in Figure 7c, are significantly lower than that obtained during the second heating run. The SAXS data obtained during heating and cooling runs at 103 °C are different, see Figure 2. These SAXS data indicate that the average grain size obtained during the cooling run are larger than those obtained during the heating run. The decrease in conductivity described above is attributed to this difference in the average grain size. After completing the cooling run, the sample was further cooled to room temperature, annealed at room temperature for two days. The sample was then subjected to the standard heating-cooling-heating protocol. The conductivity measured during the last heating step is shown by maroon stars in Figure 7c. Annealing the electrolytes at room temperature for an extended period of time (more than two days) is necessary to obtain the conductivity data reported in Figure 7a and 7b. It is evident that subtle changes in grain structure and connectivity have a significant effect on ion transport. It is also evident that the grain structure below 125 °C is a complex function of thermal history due to the semicrystalline nature of the POSS-rich microphase.

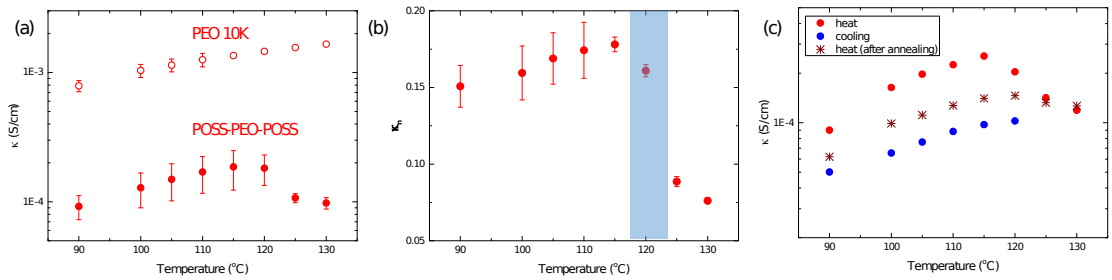

Figure 7. (a) The conductivity of the electrolytes are plotted against temperature. The open circles represent PEO and the filled circles represents the copolymer based electrolytes, respectively (b) the normalized conductivity κ_n with respect to PEO (M.W. = 10 kg/mol) is plotted against the temperature. κ_n decreases as the POSS chains melts at 117 °C (c) The temperature dependent conductivity of one of the cells is plotted. The red and blue circles represent the heating and cooling runs from first experiment and the maroon star represents the heating run after two days of annealing at room temperature. The second experiment represents slow recovery of the conductivity with time.

Conclusions

We have studied the effect of temperature on the morphology and conductivity of a POSS-PEO-POSS/LiTFSI mixture. We focus on the interplay between crystallinity of the POSS microphase and grain structure. It is important to recognise that the grain structure in two independent samples with identical thermal histories will be statistically similar but not identical. Defects and grain boundaries in such samples can be eliminated by annealing at high temperature but such changes are usually irreversible. SAXS and TEM data from our POSS-PEO-POSS/LiTFSI mixture indicate that the average grain size increases substantially when the sample is heated above 113 °C. An unusual feature of the sample is that the grain structure changes reversibly with temperature, i.e., smaller grains are obtained when the sample is cooled below 113 °C. The ionic conductivity of the electrolyte also exhibits reversible changes in this temperature window. The grain structure of our electrolyte is greatly affected by crystallization of the non-conducting POSS-rich microphase. Our work is but one

step toward a comprehensive understanding of the effect of grain structure on ion transport in microphase separated block copolymers.

Acknowledgements

Primary funding for this work was provided by the Assistant Secretary for Energy Efficiency and Renewable Energy, Office of Vehicle Technologies of the U.S. Department of Energy under Contract DE-AC02-05CH11231under the Battery Materials Research Program. The electron microscopy work was performed at Donner Lab which was provided by the Soft Matter Electron Microscopy Program (KC11BN), supported by the Office of Science, Office of Basic Energy Science, US Department of Energy, under Contract DE-AC02-05CH11231. Work at the Advanced Light Source, which is a DOE Office of Science User Facility, was supported by Contract No. DEAC02-05CH11231. Work at the Stanford Synchrotron Radiation Light Source, a user facility at SLAC National Accelerator Laboratory, was supported by the U.S. Department of Energy, Office of Science, Office of Basic Energy Sciences under Contract No. DE-AC02-76SF00515. Work at the Molecular Foundry was supported by the Office of Science, Office of Basic Energy Sciences, of the U.S. Department of Energy under Contract No. DE-AC02-05CH11231.

Abbreviations

I	scattering intensity
q	scattering vector (nm^{-1})
q^*	scattering vector at the primary scattering peak (nm^{-1})
d	domain spacing ($d = 2\pi / q^*$)
r	salt concentration ([Li]/[EO])
S	scattering invariant
f_i	volume fraction of component i
M.W.	molecular weight (kg/mol)
fwhm	full width at half maxima

Greek

ω	frequency
κ	conductivity
κ_n	normalized conductivity.

Associated content

Supporting Information. NMR, GPC, DSC, rheology, conductivity, volume fraction calculation, scattering invariant, WAXS, conductivity

Author Information

Corresponding authors

Nitash P. Balsara

*nbalsara@berkeley.edu

Irune Villaluenga

*irvillaluenga@gmail.com

Author Contributions

The manuscript was written through contributions of all authors. All authors have given approval to the final version of the manuscript.

Notes

The authors declare no competing financial interest.

References

1. Berthier, C.; Gorecki, W.; Minier, M.; Armand, M. B.; Chabagno, J. M.; Rigaud, P. Microscopic investigation of ionic conductivity in alkali metal salts-poly(ethylene oxide) adducts. *Solid State Ionics* **1983**, *11*, 91−95.

2. Bouchet, R.; Maria, S.; Meziane, R.; Aboulaich, A.; Lienafa, L.; Bonnet, J. P.; Phan, T. N. T.; Bertin, D.; Gigmes, D.; Devaux, D.; Denoyel, R.; Armand, M. Single-ion BAB triblock copolymers as highly efficient electrolytes for lithium-metal batteries. *Nat. Mater*. **2013**, *12*, 452−457.

3. Balsara, N. P.; . Newman, J. Comparing the energy content of batteries, fuels, and materials. *J. Chem. Educ*. **2013**, *90*, 446-452

4. Armand, M.; Tarascon, J. M. Building better batteries. *Nature* **2008**, *451*, 652−657.

5. Young, W. S.; Kuan, W. F.; Epps, T. H. Block copolymer electrolytes for rechargeable lithium batteries. *J. Polym. Sci., Part B: Polym. Phys*. **2014**, *52*, 1– 16

6. Singh, M.; Odusanya, O.; Wilmes, G. M.; Eitouni, H. B.; Gomez, E. D.; Patel, A. J.; Chen, V. L.; Park, M. J.; Fragouli, P.; Iatrou, H.; Hadjichristidis, N.; Cookson, D.; Sciences, M.; Di, V.; Berkeley, L. Effect of molecular weight on the mechanical and electrical properties of block copolymer electrolytes. *Macromolecules* **2007**, *40*, 4578– 4585

7. Galluzzo, M.; Loo, W. S.; Wang, A. A.; Walton, A.; Maslyn, J. A.; Balsara, N. P. Measurement of three transport coefficients and the thermodynamic factor in block copolymer electrolytes with different morphologies. *J. Phys. Chem. B* **2020**, *124*, 921-935

8. Huang, J.; Tong, Z. Z.; Zhou, B.; Xu, J. T.; Fan, Z. Q. Phase behavior of LiClO4-doped poly(ε-caprolactone)-b- poly(ethylene oxide) hybrids in the presence of competitive interactions. *Polymer (Guildf).* **2014**, *55*, 1070–1077.

9. Young, W. S.; Epps, T. H. Salt doping in PEO-containing block copolymers: Counter ion and concentration effects. *Macromolecules* **2009**, *42*, 2672–2678.

10. Zardalidis, G.; Gatsouli, K.; Pispas, S.; Mezger, M.; Floudas, G. Ionic Conductivity, self-assembly, and viscoelasticity in poly(styrene-b-ethylene oxide) electrolytes doped with LiTf. *Macromolecules* **2015**, *48*, 7164–7171

11. Naidu, S.; Ahn, H.; Gong, J.; Kim, B.; Ryu, D. Y. Phase behavior and ionic conductivity of lithium perchlorate-doped polystyrene-b-poly(2-vinylpyridine) copolymer. *Macromolecules* **2011**, *44*, 6085–6093.

12. Irwin, M. T.; Hickey, R. J.; Xie, S.; Bates, F. S.; Lodge, T. P. Lithium salt-induced microstructure and ordering in diblock copolymer/homopolymer blends. *Macromolecules* **2016**, *49*, 4839–4849.

13. Gomez, E. D.; Panday, A.; Feng, E. H.; Chen, V.; Stone, G. M.; Minor, A. M.; Kisielowski, C.; Downing, K. H.; Borodin, O.; Smith, G. D.; Balsara, N. P. Effect of ion distribution on conductivity of block copolymer electrolytes. *Nano Lett*. **2009**, *9*, 1212–1216

14. Hu, H.; Gopinadhan, M.; Osuji, C. O. Directed self-Assembly of block copolymers: A tutorial review of strategies for enabling nanotechnology with soft matter. *Soft Matter* **2014**, *10*, 3867–3889.

15. Hou, K. J.; Qin, J. solvation and entropic regimes in ion-containing block copolymers. *Macromolecules* **2018**, *51*, 7463–7475.

16. Sethuraman, V.; Mogurampelly, S.; Ganesan, V. Multiscale simulations of lamellar PS-PEO block copolymers doped with LiPF6 ions. *Macromolecules* **2017**, *50*, 4542–4554.

17. Loo, W. S.; Galluzzo, M.; Li, X.; Maslyn, J.; Oh, H. J.; Mongcopa, K. I.; Zhu, C.; Wang, A. A. Wang, X.; Garetz, B. A.; Balsara, N. P. Phase behavior of mixtures of block copolymers and a lithium Salt. *J. Phys. Chem. B* **2018**, *122*, 8065-8074

18. Sethi G. K.; Jung, H. Y.; Loo, W. S.; Sawhney, S.; Park, M. J.; Balsara, N. P. Villaluenga, I. Structure and thermodynamics of hybrid organic-inorganic diblock copolymers with salt. *Macromolecules* **2019**, *52*, 3165-3175

19. Newstein, M. C.; Garetz, B. A.; Balsara, N. P.; Chang, M. Y.; Dai, H. J. Growth of grains and correlated grain clusters in a block copolymer melt. *Macromolecules* **1998**, *31*, 64–76.

20. Ryu, H. J.; Sun, J.; Avgeropoulos, A.; Bockstaller, M. R. Retardation of grain growth and grain boundary pinning in athermal block copolymer blend systems. *Macromolecules* **2014**, *47*, 1419–1427

21. Chastek, T. Q.; Lodge, T. P. Measurement of gyroid single grain growth rates in block copolymer solutions. *Macromolecules* **2003**, *36*, 7672–7680.

22. Chintapalli, M.; Chen, C.; Thelen J. L.; Teran, A. A.; Wang, X,; Garetz, B. A.; Balsara, N. P. Effect of grain size on the ionic conductivity of a block copolymer electrolyte. *Macromolecules* **2014**, *47*, 5424-5431

23. Xie, S.; Meyer, D. J.; Wang, E.; Bates, F. S.; Lodge, T. P. Structure and properties of bicontinuous microemulsions from salt-doped ternary polymer blends. *Macromolecules* **2019**, *52*, 9693-9702

24. Young, W. S.; Epps, T. H. Ionic conductivities of block copolymer electrolytes with various conducting pathways: sample preparation and processing considerations. *Macromolecules* **2012**, *45*, 4689–4697

25. Sax, J.; Ottino, J. M. Modeling of transport of small molecules in polymer blends: application of effective medium theory. *Polym. Eng. Sci.* **1983**, *23*, 165–176.

26. Harrison, C.; Adamson, D. H.; Cheng, Z.; Sebastian, J. M.; Sethuraman, S.; Huse, D. A.; Register, R. A.; Chaikan, P. M. Mechanism of ordering in stripped patterns. *Science* **2000**, *290*, 1558– 1560

27. Ryu, H. J.; Fortner, D. B.; Lee, S.; Ferebee, R.; De Graef, M.; Misichronis, K.; Avgeropoulos, A.; Bockstaller, M. R. Role of grain boundary defects during grain coarsening of lamellar block copolymers *Macromolecules* **2013**, *46*, 204–215

28. Huang, E.; Mansky, P.; Russell, T. P.; Harrison, C.; Chaikin, P. M.; Register, R. A.; Hawker, C. J.; Mays, J. Mixed lamellar films: evolution, commensurability effects, and preferential defect formation *Macromolecules* **2000**, *33*, 80– 88

29. Sethi, G. K.; Jiang, X.; Chakraborty, R.; Loo, W. S.; Villaluenga, I.; Balsara, N. P. Anomalous self-assembly and ion transport in nanostructured organic–inorganic solid electrolytes. *ACS Macro Lett*. **2018**, *7*, 1056-106

30. Ilavsky, J. Nika: Software for two-dimensional data reduction. *J. Appl. Crystallogr*. **2012**, *45*, 324–328

31. Hosemann, R.; Bagchi, S. N. Direct Analysis of Diffraction by Matter; North-Holland: Amsterdam, **1962**.

32. Scherrer, P. Determination of the size and internal structure of colloid particles using X-rays. *Gottinger Nachrichten* **1918**, *2*, 98-100

33. Smilgies, D. M. Scherrer grain-size analysis adapted to grazing-incidence scattering with area detectors. *J. Appl. Crystallogr*. **2009**, *42*, 1030-1034

34. Wang, X.; Chintapalli, M.; Newstein, M. C.; Balsara, N. P.; Garetz, B, A. Characterization of a Block Copolymer with a Wide Distribution of Grain Sizes. *Macromolecules* **2016**, *49*, 8198-8208

35. Anh, B.; Hirai, T.; Jin, S.; Rho, Y.; Kim, K. LiuW.; Kakimoto, M.; Gopalan, P.; Hayakawa, T.; Ree, M. Hierarchical structure in nanoscale thin films of a poly(styrene-b-methacrylate grafted with POSS) (PS214-b-PMAPOSS27). *Macromolecules* **2010**, *43*, 10568–10581

36. Zhu, Y. F.; Liu, W.; Zhang, M. Y.; Zhou, Y. D.; Hou, P. P.; Pan, Y.; Shen, Z.; Fan, X, H.; Zhou, Q. F. POSS-containing jacketed polymer: hybrid inclusion complex with hierarchically ordered structures at sub-10 nm and angstrom length scales. *Macromolecules* **2015**, *48*, 2358−2366

37. Galin, M.; Mathis, A. Structural and thermodynamic study of dimethylsiloxane-ethylene oxide PDMS-PEO-PDMS triblock copolymers. *Macromolecules* **1981**, *14*, 677– 683

38. Unger, R.; Beyer, D.; Donth, E. Phase behaviour in poly(ethylene oxide-b-t-butyl methacrylate) block copolymers. *Polymer* **1991**, *32*, 3305– 3312

39. Ishikawa, S. Microphase separation and crystallization of crystalline-amorphous type block copolymer. V: Thermal reproducibility *Eur. Polym. J*. **1993**, *29*, 1621– 1624

40. Mai, S. M.; Fairclough, J. P. A.; Viras, K.; Gorry, P. A.; Hamley, I. W.; Ryan, A. J.; Booth, C. Chain folding in semicrystalline oxyethylene/oxybutylene diblock copolymers. *Macromolecules* **1997**, *30*, 8392– 8400

41. Hong, S.; Yang, L.; MacKnight, W. J.; Gido, S. P. Morphology of a crystalline/ amorphous diblock copolymer: poly((ethylene oxide)-b-butadiene). *Macromolecules* **2001**, *34*, 7009– 7016

42. Rangarajan, P.; Register, R. A.; Fetters, L. J.; Bras, W.; Naylor, S.; Ryan, A. J.; Crystallization of a Weakly Segregated Polyolefin Diblock Copolymer. *Macromolecules* **1995**, *28*, 4932-4938

43. Di Marzio, E. A.; Guttman, C. M.; Hoffman, J. D. Calculation of Lamellar Thickness in a Diblock Copolymer, One of Whose Components Is Crystalline. *Macromolecules* **1980**, *13*, 1194-1198

44. Whitmore, M. D.; Noolandi, J. Theory of crystallizable block copolymer blends. *Macromolecules* **1988**, *21*, 1482-1496

45. Rangarajan, P.; Register, R. A.; Fetters, L. J. Morphology of semicrystalline block copolymers of ethylene-(ethylene-alt-propylene) *Macromolecules* **1993**, *26*, 4640-4645

46. Adams, J.; Quiram, D. Graessley, W. W.; Register, R. A.; Marchand, G. R. Ordering dynamics of compositionally asymmetric styrene-isoprene block copolymers. *Macromolecule* **1996**, *29*, 2929–2938.

47. Li, X.; Loo, W. S.; Jiang, X.; Wang, X.; Galluzzo, M. D.; Mongcopa, K. I.; Wang, A. A.; Balsara, N. P.; Garetz, B. A. Confined versus unconfined crystallization in block copolymer/salt mixtures studied by depolarized light scattering. *Macromolecules* **2019**, *52*, 3, 982-991

48. Loo, W. S.; Mongcopa, K, I.; Gribble, D. A.; Faraone, A. A.; Balsara, N. P. Investigating the Effect of Added Salt on the Chain Dimensions of Poly(ethylene oxide) through Small-Angle Neutron Scattering. *Macromolecules* **2019**, *52*, 8724−8732

49. Li, S.; Myers, S. B.; Register, R. A.; Solid-State Structure and Crystallization in Double-Crystalline Diblock Copolymers of Linear Polyethylene and Hydrogenated Polynorbornene. *Macromolecules* **2011**, *44*, 8835–8844

50. Beckingham, B. S.; Register, R. A. Architecture-Induced Microphase Separation in Nonfrustrated A−B−C Triblock Copolymers. *Macromolecules* **2013**, *46*, 3486−3496

51. Burns, A. B.; Register, R. A. Large, Reversible, and Coherent Domain Spacing Dilation Driven by Crystallization under Soft Lamellar Confinement. *Macromolecules* **2017**, *50*, 8106−8116

52. Zhu, L.; Cheng, S. Z. D.; Huang, P.; Ge, Q.; Quirk, R. P.; Thomas, E. L.; Lotz, B.; Hsiao, B. S.; Yeh, F.; Lui, L. Nanoconfined Polymer Crystallization in the Hexagonally Perforated Layers of a Self-Assembled PS-b-PEO Diblock Copolymer. *Adv. Mater*. **2002**, *14*, 31-34

53. Chatterjee, J.; Jain S.; Bates, F. S. Comprehensive Phase Behavior of Poly(isoprene-b-styrene-b-ethyleneoxide) Triblock Copolymers. *Macromolecules* **2007**, *40*, 2882-2896